LAWRENCE
LIVERMORE
NATIONAL
LABORATORY

LLNL-JRNL-421389

X-ray Absorption Spectroscopy Characterization of Zn Underpotential Deposition on Au(111) from Phosphate Supporting Electrolyte

J. R. Lee, R. L. O'Malley, T. J. O'Connell, A. Vollmer, T. Rayment

December 14, 2009

Electrochimica Acta

Disclaimer

LLNL-JRNL-421389

X-ray Absorption Spectroscopy Characterization of Zn Underpotential Deposition on Au(111) from Phosphate Supporting Electrolyte

Jonathan R.I. Lee[1,2,†], Rachel L. O'Malley[1], Timothy J. O'Connell[1]
Antje Vollmer[1,3], Trevor Rayment[1,4,*]

[1] Department of Chemistry, University of Cambridge,
Lensfield Road, Cambridge, CB2 1EW, UK

[2] Lawrence Livermore National Laboratory, Livermore, CA 94550, USA

[3]Helmholtz Zentrum Berlin f. Materialien und Energie, BESSY II,
Albert-Einstein-Str. 15, 12489 Berlin, Germany
[4]Diamond Light Source Ltd., Diamond House, Harwell Science and Innovation Campus,
Didcot, Oxfordshire OX11 0DE, UK

[†]lee204@llnl.gov, *trevor.rayment@diamond.ac.uk

August 10, 2010

Abstract

Zn K-edge X-ray absorption spectroscopy (XAS) has been used to investigate the structure of Zn monolayers prepared on Au(111) electrodes via underpotential deposition (UPD) from phosphate supporting electrolyte. Theoretical modeling of the XAS data indicates that the Zn adatoms adopt a commensurate ($\sqrt{3}$x$\sqrt{3}$)R30° (θ_{sc}=0.33) adlayer structure and reside within the 3-fold hollow sites of the Au(111) surface. Meanwhile, phosphate counter-ions co-adsorb on the UPD adlayer and bridge between the Zn adatoms in a ($\sqrt{3}$x$\sqrt{3}$)R30° (θ_{sc}=0.33) configuration, with each phosphorous atom residing above a vacant 3-fold hollow site of the Au(111). Significantly, this surface structure is invariant between the electrochemical potential for UPD adlayer formation and the onset of bulk Zn electrodeposition. Analysis of the Zn K-edge absorption onset also presents the possibility that the Zn adatoms do not fully discharge during the process of UPD, which had been proposed in prior voltammetric studies of the phosphate/Zn(UPD)/Au(111) system.

1 Keywords

Underpotential deposition, XAS, Zinc, Phosphate, Au electrode

2 Introduction

Underpotential deposition (UPD), the phenomenon of metal monolayer formation on a foreign metal substrate under more oxidizing potentials than the equilibrium potential for bulk electrodeposition, has been the subject of considerable research in recent years because it yields model systems for investigation of the electrode/electrolyte interface [1, 2, 3, 4]. Many UPD systems are composed of well-ordered adlayers that are commensurate with the underlying electrode surface and, as such, offer an excellent opportunity to study the structure and composition of the interfacial region. Furthermore, they enable the evaluation and comparison of different techniques for structural characterization of the electrified interface. The capability for analysis of the interfacial structure is of fundamental importance in developing an enhanced understanding of the modes and mechanisms of electrochemical surface processes and, therefore, insight into technologically relevant procedures such as electroplating and electrocatalysis. In this paper, X-ray absorption spectroscopy (XAS) is used to characterize the structure of Zn monolayers prepared on Au(111) substrates via UPD from phosphate supporting electrolyte.

XAS provides a valuable technique for structural analysis of the electrified interface. The elemental specificity of XAS enables one to characterize the local environment (up to a radius of $\sim$ 5 Å [5, 6]) of individual elements within a condensed phase and, as such, allows the detailed investigation of both ordered and amorphous systems. Therefore, XAS represents a complementary or alternative tool to techniques that require longer range order, which include X-ray diffraction (XRD)/surface X-ray scattering (SXS). One can also conduct in situ XAS measurements of electrode materials with the use of synchrotron radiation [7, 8, 9], including in situ structural studies of the electrode surface [10, 11, 12, 13]. This is an important capability because it eliminates the potential for rearrangement of the interfacial structure upon removal of the working electrode from the electrolyte and, by extension, electrochemical control. Despite the apparent strengths of XAS for investigation of the electrode surface structure, use of the technique to study UPD systems was largely discontinued after the late 1990's because of the extended data collection periods required to obtain high quality spectra. Significantly, a recent study of electrodeposited Cu monolayers on Au from sulfate buffer illustrates that improvements in flux and detection efficiency at synchrotron sources has mitigated this problem for UPD adlayers with high surface coverages (surface coverage, θ_{sc}, $\geq$0.67) [13]. Zn UPD on Au(111) from phosphate buffer is an excellent system with which to build upon this preceding Cu(UPD)/Au(111) study for several reasons: (1) voltammetric experiments indicate that the Zn adlayer has a considerably reduced surface coverage ($\theta_{sc}\sim$0.33) [14, 15, 16] with respect to Cu UPD and, therefore, provides an opportunity to demonstrate the suitability of XAS for the investigation of low concentration surface species; (2) the specific geometrical arrangement of the Zn adlayer and co-adsorbed anion overlayer remains unresolved, despite prior research conducted for the phosphate/Zn(UPD)/Au(111) system using a range of characterization techniques; (3) the mechanisms of Zn electrodeposition and structure of the resulting deposit are of relevance for important industrial applications, particularly in understanding the formation and properties of anti-corrosion galvanic coatings. In fact, interest in the processes of Zn electrodeposition has resulted in studies of Zn UPD on a variety of metal electrodes that include Au [2, 14, 15, 17, 16, 18, 19, 20, 21, 22], Pd [23, 24], Pt [23, 24, 25, 26, 27, 28, 29, 30, 31, 32, 33], Ag [34], Cu [19] and Cd [19].

Although the experiments reported to date do not yield a definitive assignment of the interfacial structure for the phosphate/Zn(UPD)/Au(111) system, they provide an excellent point of reference and offer invaluable information to assist in an XAS investigation. In particular, in situ scanning tunneling microscopy (STM) images recorded by Nakamura and co-workers [14, 17] display a ($\sqrt{3}$x$\sqrt{3}$)R30° (θ_{sc}=0.33) arrangement of atoms with respect to the underlying Au(111) surface that the authors attribute to phosphate anions co-adsorbed on the Zn adlayer. The structure of the UPD monolayer could not be resolved from the STM micrographs, but a tentative 2D arrangement of the interfacial region was

proposed in which the Zn adatoms bridge between at least two Au atoms at the electrode surface. Meanwhile, individual phosphate counter-ions co-adsorb at different heights above the plane of the Zn UPD adlayer within the model.

The XAS investigation of the phosphate/Zn(UPD)/Au(111) system presented in this study addresses numerous aspects of the interfacial structure that were previously unresolved. Modeling of the experimental XAS spectra yields the structure of the Zn adlayer buried beneath the co-adsorbed phosphate counter-ions and the registry between the UPD adlayer and anionic overlayer. The timescales required to obtain spectra with a sufficient signal to noise (S/N) ratio for extended analysis are shown to be competitive to alternative x-ray based characterization techniques, such as SXS/XRD, and, therefore, suitable for routine studies of low concentration surface species using synchrotron radiation.

2.1 Reagents and Materials

All reagents were obtained from commercial sources and used without further purification. Boron nitride (99%), potassium dihydrogen phosphate (99.99%), zinc oxide (99.99%) and zinc perchlorate (99.99+%) were purchased from Aldrich. 5μm zinc metal foil, 3μm thick Mylar film and 5μm Kapton film were purchased from Goodfellow. Tempax glass was purchased from UQG Optics Ltd. The Au beads (99.99%) used in preparation of the evaporated thin film Au(111) working electrodes (WEs) and the Pt foil(99.99%) used as the counter electrode (CE) were obtained from Birmingham Metal. The reference electrode (RE) was a saturated calomel electrode (SCE, REF401) purchased from Radiometer. All potentials in this manuscript are reported with respect to SCE.

2.2 Preparation of the Working Electrode, Electrolyte and XAS Standards

The WEs were prepared by thermal evaporation of Au onto a Tempax glass substrate. Each substrate was machined from 5 mm thick plate to yield an upper surface that is comprised of two ends chamfered at 45° to a flat and polished plane of dimensions 18x24 mm. When coated with Au, this plane provides the WE surface studied with XAS. Meanwhile, Au deposited on the sloping faces allows for direct electrical contact to the WE without incurring any surface damage. Rigorous cleaning of the glass was undertaken prior to Au deposition. Initially, the substrates were immersed in aqua regia (3:1 ratio of concentrated HCl:HNO_3) for ∼60s to remove any existing Au film and then rinsed in ultrapure water (Elga, 18.2MΩcm). Subsequent agitation in piranha solution (3:1 ratio of H_2SO_4:H_2O_2) for ∼1hr served to remove organic contaminants from the substrates [35]. After a second phase of rinsing in ultrapure water, the samples were dried in N_2 and immediately transferred to the evaporation chamber (Balzer UTT440).

Once secured within the evaporation chamber, the substrates were preheated at ∼300°C for 10 hrs and then coated with 1500Å Au at a rate of 1Å/s and a chamber pressure of ∼1x10^{-6}torr. Upon reaching the required thickness of Au deposit, the samples were annealed at ∼300°C for 6 hours to yield domains with a (111) surface orientation and to achieve a comparable surface roughness to Au films prepared on mica [36]. Following the annealing phase, the samples were slowly cooled to room temperature over a 10hr period, to prevent film fracture under the stresses of rapid temperature change.

All electrolytes were prepared in ultrapure water and composed of 0.1-1mM $Zn(ClO_4)_2$ and 0.1M KH_2PO_4 (pH 4.4-4.5). Dissolved molecular oxygen was removed from the electrolytes by purging with Ar for ≥30 min before each experiment. For the purposes of reference and comparison, three Zn containing standards were prepared for XAS measurement in the transmission mode. The 5μm Zn metal foil was mounted in a suitable frame without further modification. Finely ground samples of ZnO were mixed with BN and pressed into pellets. The concentration of BN in each pellet was adjusted until an absorption of μt∼1 was achieved. Finally, a 10mM aqueous solution of $Zn(ClO_4)_2$ was prepared and transferred to a liquid cell with a 2 mm path length for transmission XAS measurements.

2.3 Instrumentation

XAS and electrochemical measurements were conducted using a purpose built cell, which was designed for use in the thin layer configuration employed by Samant *et al.* [37] for SXS studies of UPD. A thorough description of the composition and operation of an equivalent cell during electrochemical and XAS studies of UPD adlayers is available in the literature [13]. We note, however, that the cell allows for exposure of the Au(111) electrodes to bulk electrolyte during electrochemical measurements and UPD adlayer deposition. Moreover, the WE faces a Mylar window, which is deflated during XAS measurements to trap a thin layer of solution at the Au(111) surface. The presence of the thin layer ensures electrochemical control over the system throughout the XAS studies, while ensuring minimal attenuation of the incident X-ray beam by the electrolyte. Electrochemical control of the system under investigation was provided by an Eco-Chemie PGSTAT12 potentiostat, which was operated using the General Purpose Electrochemical System (GPES) software, and a standard three-electrode configuration comprising of the Au(111) WE, Pt foil CE and SCE RE. The preparation and XAS measurement of a surface adlayer of Zn was conducted at a constant electrode potential within the appropriate region for UPD. During adlayer formation, the experimental cell was held in the fully inflated configuration for 20 min to ensure that an equilibrium surface coverage was reached. The Mylar film was then deflated and the cell transferred to the experimental beamline without loss of the potentiostatic condition.

XAS measurements were conducted on Station ID26 at the European Synchrotron Radiation Source (ESRF), Grenoble, France. A detailed description of the beamline and storage ring properties during the course of this study are available in the literature [13]. The energy of the incident X-ray photons was calibrated to the maximum in the first derivative of the XAS spectrum obtained from the 5μm zinc metal foil. An ionization chamber was utilized for the measurement of I_0 and a photodiode detector positioned behind the experimental sample provided I_t. Measurements in the fluorescence mode were conducted using a solid state 13-element Ge detector array (Canberra). The detector permitted count rates of up to 100 kHz with deadtime correction and offered a resolution of $\sim$300eV FWHM for the Zn K_α fluorescence photons.

All fluorescence XAS measurements were conducted on ID26 using a single experimental geometry. In this configuration, the fluorescence detector was mounted in the horizontal plane at an angle of 90° with respect to the axis of the incident beam. The active surface of the detector was covered by a Z-1 filter (Cu, 5μm thick) to reduce the background signal obtained from Compton and elastic scattering [38]. In addition to improving the ratio of S/N, this allowed a closest approach of 5 to 6 cm between sample and detector without saturation of the device. The cell was mounted on the experimental beamline by means of a motorized goniometer (ID26) such that the electric vector of the incident radiation was perpendicular to the Au(111) surface plane of the WE. The angle of incidence, α, between the X-ray beam and sample surface was selected to approach grazing incidence as closely as possible but was ultimately limited to α=5° by the relative dimensions of the WE surface and cross-section of the beam. Individual spectra were collected over a 35 to 40 min period and a spectral range of 9500 to 10150 eV. Those recorded under identical experimental conditions, typically 2-3 spectra, were combined to provide an improvement in S/N.

2.4 Analysis

Initially, raw XAS data was extracted from the native beamline data format using SPEC and XOP. The energy of the absorption edge, E_0, was identified by the maximum in the first derivative of XAS spectra collected from the 5μm Zn foil. All spectra were normalized to I_0 and, subsequently, to the magnitude of the edge step, which was taken to be the difference in absorption intensity between the pre-edge region and 50 eV beyond the absorption edge. Extraction of the EXAFS via subtraction of the pre- and post-edge backgrounds was conducted using PAXAS [39]. The pre-edge region was modeled using a second order polynomial and the post-edge region was mod-

eled with a cubic spline, which was refined via a least squares fitting routine. The Cook-Sayers criterion [40] was applied as an important diagnostic throughout the process of background subtraction.

For the purposes of structural analysis, theoretical modeling of the experimental EXAFS was conducted using EXCURV98 [41]. The fit parameter, R, provides a measure of the match between the experimental and theoretical spectra and is defined by:

$$R = \sum_{i}^{N} (\frac{1}{\sigma_i})[|\chi_i^e(k) - \chi_i^t(k)|].100\% \qquad (1)$$

where ${\chi_i}^e(k)$ represents the experimental EXAFS, ${\chi_i}^t(k)$ represents the theoretical EXAFS derived from the structural model, σ_i represents a weighting parameter at point i and N is the total number of data points in the spectrum. An improvement in fitting is accompanied by a reduction in R and, as a consequence, structural refinement using EXCURV98 was conducted with the intent of minimizing this parameter, while also ensuring that the model was chemically and physically viable. The model development was carried out according to established protocols that are described in greater detail in the literature [13, 41]: the theoretical structure is refined to optimize R after the inclusion of each 'shell' of symmetry-related atoms, which are added sequentially in order of proximity to the absorbing atom (shells at comparable distances were added simultaneously).

The position of each backscattering atom is defined relative to the absorbing element using a spherical polar co-ordinate scheme. Within this scheme, the colatitudal angle, θ, is measured with respect to the Au(111) surface normal and has a range of $0 \leq \theta \leq 180°$, the azimuthal angle, ϕ, resides in the plane of the WE surface and has a range of $0 \leq \phi \leq 360°$ and the distance, r, represents the interatomic separation. In addition, the atoms contained in an individual shell are described collectively by their number, n, element type, t, and relevant Debye-Waller factor (second cumulant), a. Therefore, a total of six degrees of freedom, or relevant independent points, are required for the characterization of each model shell.

The number of relevant independent points, N_I, available for modeling was calculated using equation 2, which was first reported by Stern [38]:

$$N_I = \frac{2\Delta r \Delta k}{\pi} + 2 \qquad (2)$$

where Δk is the range in k-space over which the spectrum is analyzed and Δr is the range in real space encompassed by the theoretical model. Structural modeling was conducted almost exclusively within the limit imposed by N_I. Additional models that did not meet this criterion were also considered, provided N_I was within six relevant independent points (i.e. a fraction of a single shell) of encompassing the entire structure, although the conclusions drawn from full refinement were treated with appropriate caution. The limits of Δk were established prior to modeling by truncation of the background subtracted data. The minimum in k was defined by the beginning of the EXAFS, while the maximum in k corresponded to the energy at which the noise and amplitude of the oscillations reached a comparable magnitude.

All data was phaseshift corrected and is presented accordingly throughout this study. The theoretical atomic phaseshifts and 'muffin-tin' potentials for each structural arrangement were calculated within EXCURV98 (using the parameters outlined in the Supporting Information). The effects of multiple scattering and, for structures of defined orientation, polarization dependence were included in all modeling.

3 Results & Discussion

3.1 Electrochemical Measurements

Figure 1 displays a characteristic CV recorded for the UPD of Zn on Au(111) from an electrolyte composed of 1mM $Zn(ClO_4)_2$ and 0.1M KH_2PO_4. Obtaining a cyclic voltammogram of the form presented in figure 1 was indicative of a well-prepared sample and provided an important system diagnostic prior to the collection of any XAS data. The appearance of the CV is consistent with those reported in the literature[14, 15, 16, 17, 18] and, as a consequence, the peaks denoted A and A^* are attributed to the

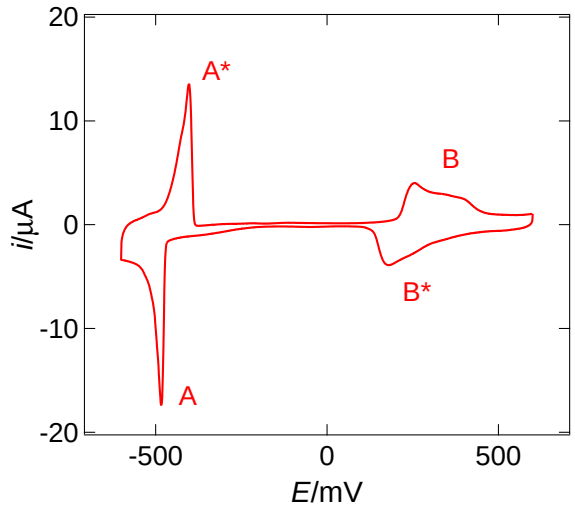

Figure 1: CV recorded for Zn UPD on Au(111) from a phosphate supporting electrolyte using a dedicated electrochemical cell with the 'hanging meniscus' configuration. CVs recorded using the XAS cell were closely comparable despite the fact that it does not contain an idealized geometrical arrangement of the 3-electrode system. As such, the CV provides an excellent point of reference for subsequent XAS studies. Electrolyte composition: 0.1 mM $Zn(ClO_4)_2$, 0.1M KH_2PO_4, Rate: $20mVs^{-1}$.

UPD adsorption and desorption of Zn respectively. Peaks B and B* are observed even in the absence of Zn and are assigned respectively to the adsorption and desorption of phosphate ions on the WE surface [14, 15, 16]. In situ TEM measurements reported by Nakamura and co-workers indicate that neither Zn nor phosphate ions are strongly adsorbed on the Au(111) surface at -200mV vs SCE and, based on this observation and the form of the cyclic voltammogram, the authors suggest that no specifically adsorbed species are present on the electrode surface in the double layer region between peaks A and B* [14]. This does not preclude the possibility that Zn adatoms could adsorb on the Au surface between -200mV vs SCE and the onset of peak A (the shoulder observed at the most oxidizing potential encompassed by peak A, $\sim$ -250 mV) without any associated reductive charge transfer.

A detailed analysis of the voltammetric data collected in this study for the phosphate/Zn(UPD)/Au(111) system is not presented in this paper since thorough treatments are available in the literature [14, 15, 16, 18]. It is important to note, however, that voltammetric measurements conducted in preparation for the XAS experiments yielded data in close qualitative and quantitative agreement with the published studies. Most significantly, experiments specifically modeled after the work of Aramata and co-workers [14, 15, 16, 18] to identify the shift in electrochemical potential of peak A (E_{UPD}) as a function of the Zn^{2+} concentration within the electrolyte yielded equivalent results: the evolution in (E_{UPD}) with [Zn^{2+}] was consistent with an overall charge transfer of ~ 1 e^- for the combined process of Zn UPD adsorption and co-adsorption of phosphate. Such close similarity in the cyclic voltammetry data ensures that the information obtained from subsequent XAS measurements can be directly compared with prior research published for the phosphate/Zn(UPD)/Au(111) system.

3.2 X-ray Absorption Spectroscopy Measurements

Zn adlayers were prepared for XAS measurements at a series of potentials (-612, -625 and -650 mV vs SCE)

between the conditions required for UPD and bulk electrodeposition. As a consequence, analysis of the XAS spectra enables an assignment of any structural evolution in the Zn adlayer and the co-adsorbed phosphate overlayer as a function of the applied potential. XAS spectra were also recorded at 500mV, where one would not anticipate the formation or presence of a Zn UPD adlayer. Instead, the Zn XAS signal should arise solely from the thin layer of solution trapped above the electrode surface. Since the number of Zn K_α fluorescence photons corresponding to the edge step is directly proportional to the concentration of Zn in the beam, the measurement at 500mV provides a quantitative assignment of the contribution from the thin layer of solution to the UPD spectra. Comparison between the fluorescence signals collected at 500mV and within the UPD region under identical experimental geometries indicates that the thin layer of Zn accounts for 4-7% of the total signal for each 'UPD' spectrum. Subtraction of the electrolyte signal did not have an appreciable effect on modeling of the UPD EXAFS in EXCURV98.

3.2.1 XANES Measurements

Figure 2 displays the XANES region of XAS spectra recorded for UPD adlayers prepared via polarization in potential at -612mV, -625mV and -650mV vs SCE for 20 min and two of the experimental standards. The close similarity between the 'UPD' XANES data provides a preliminary, although not conclusive, indication that the structure of the Zn adlayer is largely constant between -612mV and -650mV vs SCE. Equally, the contrasting shape and energy of absorption onset with respect to the experimental standards illustrates that the 'UPD' XAS signals do not arise from the formation of bulk Zn deposit or primarily from the thin layer of Zn^{2+} in solution. The absorption edge for the UPD spectra (9662 eV) resides between the values for the bulk Zn metal (Zn^0, 9659 eV) and the Zn^{2+} solution (9664 eV), which presents the possibility that the Zn adatoms do not fully reduce during the process of adsorption and support an intermediate oxidation state in the region of $\sim +1$, a feature that has also been proposed for Cu UPD on Au electrodes from sulfate

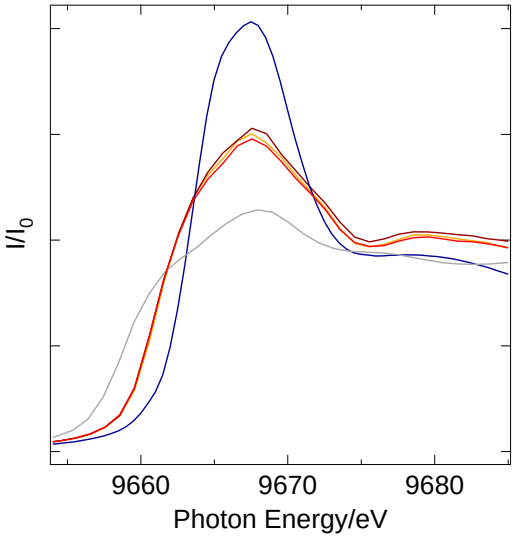

Figure 2: Individual XANES spectra recorded at the Zn K-edge for a Zn UPD monolayer prepared on Au(111) from phosphate supporting electrolyte at -612mV (orange), -625mV (red) and -650mV (dark red) vs SCE region, Zn metal (grey) and Zn^{2+} in aqueous solution (blue). All of the spectra are pre-edge background subtracted and normalized to the edge step.

supporting electrolyte [42, 43, 44]. A definitive assignment of the oxidation state cannot be obtained from inspection of the XANES and comparison with standard spectra alone because changes in the local environment of Zn can lead to modifications in the occupied and unoccupied electronic density of states and shifting of the absorption edge, without any variation in oxidation state. In fact, ex situ X-ray photoelectron spectroscopy studies indicate small shifts (<1 eV) in the binding energy of core electrons within the adatoms of Cu(UPD)/Au(111) [45] and Ag(UPD)/Au(111) [46] systems with respect to bulk Cu and Ag, which are attributed to the effects of adatom-substrate interactions (e.g. orbital expansion/contraction resulting from the size mismatch between the Cu or Ag and Au). There is also well established discussion in the community on the effect of charge rearrangement arising from the difference in workfunction/electronegativity of substrate and adsorbate as demonstrated by Trasatti [47] and Kolb et al. [48, 1, 49]. This charge transfer might well cause ionic Zn species at the surface or result in the formation of a dipole.

Even so, the possibility that the Zn adatoms retain an intermediate charge in the region of +1 is intriguing because voltammetric studies demonstrate that the UPD of Zn on Au(111) [18] and polycrystalline Au electrodes [22] from phosphate buffer is a one electron transfer process. Furthermore, the authors could not unambiguously attribute an oxidation state of +1 to the Zn adatoms from voltammetric analysis alone due to the potential for charge transfer between the co-adsorbed phosphate ions and the UPD adlayer. For an oxidation state of +1 (i.e. the one electron transfer is between the Au surface and a Zn adatom), the charge density associated with the Zn adsorption (peak A) in the cyclic voltammogram corresponds to a surface coverage of $\theta \sim 0.3$, which is within experimental error of the coverage ($\theta \sim 0.33$) predicted by Nakamura and co-workers and [14] acts as a guide for subsequent structural modeling of the XAS.

3.2.2 EXAFS Measurements

As an initial diagnostic of the background subtraction and modeling procedures, EXAFS spectra recorded for the experimental standards were fitted with well-characterized crystallographic/local structures (e.g. an hcp arrangement for Zn metal, the wurtzite structure of ZnO and octahedrally co-ordinated Zn^{2+} in aqueous solution). High quality fits of $R \leq 30\%$ were obtained for all of the standard materials. Each of the standard structures was also applied in modeling of the experimental EXAFS recorded for the Zn UPD adlayers. These models resulted in extremely poor ($R \geq 70\%$) fits, which indicates that undesired solids, such as Zn metal and ZnO, are not responsible for the XAS spectra between -650mV$\leq E \leq$-612mV and provides additional confirmation that the contribution from solvated Zn^{2+} to the EXAFS signal is low.

Subsequent models applied to the EXAFS spectra recorded for the UPD adlayers were based upon Zn adsorption in the atop, 2-fold bridging and 3-fold hollow sites of an Au(111) surface. Deviation from an idealized Au(111) surface and from perfect registry of the Zn adatoms within each adsorption site was accommodated during model refinement, provided that the structure remained physically viable. A range of configurations for anions within the co-adsorbed overlayer were also included as essential components of the model structures. The best-fitting model was identical for the Zn adlayers prepared between -650mV$\leq E \leq$-612mV, which indicates that the local environment of the adatoms remains unchanged within this region of electrochemical potential. Hence, modeling in EXCURV98 is discussed collectively for EXAFS recorded at all three 'UPD' potentials in the following discussion.

Figure 3(a) displays a comparison between a representative EXAFS spectrum collected within the UPD region and the best fitting model obtained in EXCURV98. Associated Fourier transforms for the experimental and theoretical EXAFS are presented in figure 3(b). In all cases, the lowest fit parameters ($R \sim 39\%$) for the 'UPD' spectra were obtained using models based upon Zn adsorption within the 3-fold hollow sites of the Au(111) electrode surface. Models based upon adsorption in the atop and 2-

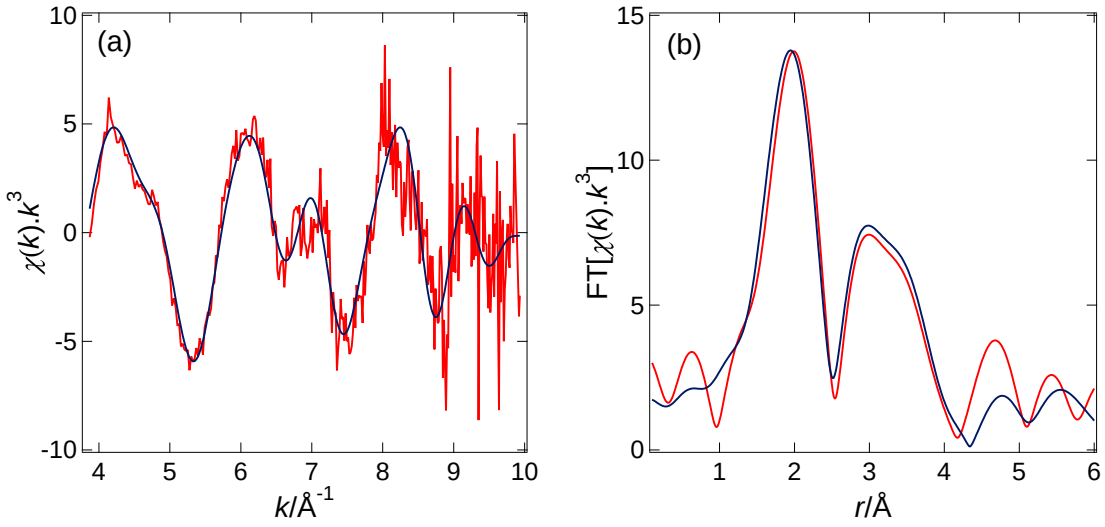

Figure 3: **(a)** A characteristic Zn K-edge EXAFS spectrum (k^3 weighted) recorded for a Zn UPD monolayer prepared in phosphate supporting electrolyte between -612 and -650 mV vs. SCE (red) and the associated best fitting theoretical model obtained using EXCURV98 (dark blue). **(b)** The corresponding FTs for the experimental EXAFS from the Zn adlayer (red) and the best fitting theoretical model (dark blue).

fold bridging sites resulted in lower quality fits to the experimental data (R∼45% and ∼43% respectively). Moreover, the corresponding local environments for Zn adsorbed in the atop and 2-fold bridging positions were inconsistent with the formation of an ordered UPD adlayer and anion overlayer (including the ($\sqrt{3}$x$\sqrt{3}$)R30° arrangement observed with in situ TEM [14, 17]) and/or with a Zn surface coverage of θ_{sc}∼33% identified via voltammetric measurements [14, 15, 16].

Structural parameters for the best fitting theoretical model of the experimental EXAFS are included in Table 1 and corresponding schematics for the local environment of the Zn adatoms viewed along multiple and distinct axes are displayed in figures 4(a) through (d). The first shell of backscatterers is composed of three oxygen atoms, which exhibit 3-fold symmetry about an axis co-incident with the Au surface normal that passes through the center of the Zn adatom. The oxygens are located above the Au atoms that directly co-ordinate to the Zn and, as such, mirror the 3-fold hollow adsorption site in which the adatom resides. Each oxygen is bonded to a distinct phosphorous atom, which indicates that three co-adsorbed counter-ions are associated with the Zn. Importantly, the projection of the Zn-O-P linkage in the plane of the Au surface is not linear: an improvement of $\Delta R \geq 1$ in the fit parameter was obtained when the P atoms were rotated by ϕ=20-30° with respect to the orientation of the Zn-O bond. The combination of this rotation with an interatomic separation of r=3.28-3.36Å and colatitudal angle of θ=54.5° places the P atoms directly above 3-fold hollow sites in the Au(111) surface that are unoccupied by the Zn adatoms. It is noteworthy that the Zn-P and Zn-Au (second shell) interatomic separations are similar (3.28-3.36Å and 2.86-2.92Å respectively), which results in the apparent asymmetry observed for the peak centered at ∼2.9Å in the FT of the experimental EXAFS (figure 3(b)) and the presence of a shoulder at ∼3.3Å.

When projected across the surface of the Au(111) electrode, the best fitting local environment of the Zn adatoms is consistent with formation of the interfacial structure displayed in Figure 4(e). The Zn adatoms form a commensurate ($\sqrt{3}$x$\sqrt{3}$)R30° monolayer structure within this arrangement, which supports an ordered overlayer of co-adsorbed counterions. Furthermore, each phosphate anion bridges between three Zn adatoms such that they also adopt a ($\sqrt{3}$x$\sqrt{3}$)R30° configuration with respect to the underlying Au electrode. The assignment of this XAS-derived surface structure is particularly interesting because it is consistent with accepted compositional and structural information for the phosphate/Zn(UPD)/Au(111) system obtained via alternative techniques: (1) the adlayer exhibits the surface coverage of Zn (θ_{sc}=0.33) reported for the phosphate/Zn(UPD)/Au(111) system in prior voltammetric studies [14, 15, 16] and (2) the ($\sqrt{3}$x$\sqrt{3}$)R30° arrangement of co-adsorbed anions is consistent with the structure observed with in situ STM [14, 17]. The agreement with prior studies lends support to the commensurate Zn adlayer arrangement obtained from the experimental EXAFS and reaffirms the value of the technique for investigating the composition and structure of the electrified interface.

Analysis of the interatomic separations for the first two shells of backscatterers provides additional insight into the experimental system. In the event that the Zn adatoms do not reduce to Zn^0 and retain a positive oxidation state within the UPD adlayer, the 1.94-1.99Å separation exceeds the anticipated bond length for the first shell of backscatterers (Zn^+-O ∼1.7Å) and would suggest that each of the three oxygen atoms directly bonded to a Zn adatom support a degree of negative charge. Given that the phosphorous atom of each counter-ion bridges between three of these oxygen atoms, a corresponding charge would be associated with the co-adsorbed phosphate ions. The interatomic separation for the second shell of backscatterers (the first Au shell, r=2.86-2.92Å) is also indicative of excess electron density associated with the backscattering Au atoms, provided the Zn adatoms retain a positive oxidation state. An excess of negative charge at the electrode surface would present the possibility that the (23x$\sqrt{3}$) reconstruction of the Au(111) surface observed [50, 51, 52, 53] in the absence of Zn is not lifted during Zn UPD.

Expanding the structural model to include additional shells of backscattering atoms would, in principle, enable further study of any surface reconstruc-

shell	atom type	number, n	radial distance, r (Å)	Debye-Waller factor, a (Å^2)	θ (°)	ϕ (°)
1	O	3	1.94-1.99	0.018-0.025	42-49	0, 120, 240
2	Au	3	2.86-2.92	0.023-0.031	135-143	0, 120, 240
3	P	3	3.27-3.35	0.012-0.026	49-57	30, 150, 270
4	Au	3	4.03-4.15	0.022-0.029	124-136	60, 180, 300
Ef	-5 to 2					

Table 1: Structural parameters for the best fitting models of the local environment of Zn atoms within the UPD monolayers prepared on Au(111) obtained from EXAFS collected between -612 and -650 mV vs. SCE.

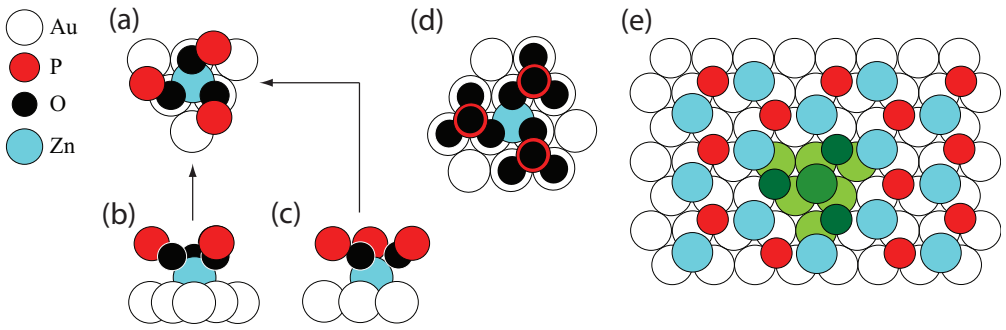

Figure 4: **(a)** A schematic of the local environment of Zn adatoms within the UPD adlayer prepared on Au(111) from phosphate supporting electrolyte viewed along the Au(111) surface normal. Note that this structure contains only the atoms included in the best-fitting structural model applied to the experimental EXAFS. **(b)** A schematic of the same local environment of Zn viewed along the plane of the Au(111) surface. **(c)** Another in-plane schematic in which the view is rotated by 90° with respect to the view in **(b)**. **(d)** A projection of the local environment displayed in **(a)** assuming that the electrode surface has a well-ordered Au(111) arrangement and that the oxygen atoms in the phosphate ions form a tetrahedral arrangement around the central phosphorous atom. **(e)** The projection of this local environment over the Au(111) surface (the oxygen atoms have been omitted for clarity in this schematic) to yield the open ($\sqrt{3}$x$\sqrt{3}$)R30° Zn adlayer with a co-adsorbed open ($\sqrt{3}$x$\sqrt{3}$)R30° overlayer of phosphate. The green atoms represent the local environment of the Zn adatoms identified via theoretical modeling of the Zn K-edge EXAFS

tion upon formation of the Zn adlayer, since one could determine the registry between the top two layers of Au atoms within the electrode. A thorough examination of this phenomenon is precluded for the data presented herein due to the limitations imposed by the N_I: at a minimum, an additional shell of Au atoms is required to model adsorption in the fcc or hcp sites of Au(111) or the 3-fold hollow sites of a reconstructed electrode surface and the associated increase in degrees of freedom exceeds the available N_I from the truncated EXAFS. Nevertheless, only a small increase in Δk and, therefore, S/N, would be necessary for the requisite improvement in N_I to model the fifth shell of atoms. The gain in S/N obtained following the combination of two or three spectra indicates that the desired improvement would be achieved via an additional $\sim$ 2 hrs of data collection ($\sim$ 4 hrs total). It is important to emphasize, however, that in the absence of this additional data collection, the combination of only three XAS spectra ($\sim$ 2 hrs total) was required for assignment of the local environment about the Zn adatoms with sufficient extent and detail to determine the structure of the UPD adlayer and co-adsorbed overlayer of counter-ions.

The 2-4 hr period required to record spectra of sufficient quality for detailed characterization of the Zn(UPD)/Au(111) system is in accordance with the preceding study of Cu UPD on Au(111) [13], in which a reduced ($\geq$ 80 min) timeframe was necessary for structural analysis of UPD monolayers with 2-fold (θ_{sc} = 0.67) or 3-fold (θ_{sc} = 1) higher surface concentrations of the metal adatoms. Meanwhile, even the upper bound of 4 hrs data collection necessary for extended analysis is competitive with alternative or complementary techniques, such as XRD/SXS, and also represents a reasonable timeframe for the routine use of synchrotron facilities.

4 Conclusions

In situ XAS measurements conducted at the Zn K-edge enable assignment of the local environment of Zn adatoms on Au(111) electrodes prepared by UPD from phosphate buffer. The structural arrangement around the Zn is invariant over a wide potential range within the UPD region. Projection of this arrangement across the Au electrode indicates that the UPD adlayer adopts a commensurate ($\sqrt{3}$x$\sqrt{3}$)R30° (θ_{sc}=0.33) arrangement on the underlying Au surface, with the Zn adatoms located in three fold hollow adsorption sites. Analysis of the XAS-derived local environment also demonstrates that the co-adsorbed layer of counter-ions adopt a ($\sqrt{3}$x$\sqrt{3}$)R30° (θ_{sc}=0.33) structure, in which each phosphate ion bridges between three Zn adatoms and the central phosphorous atom resides above a vacant 3-fold hollow site on the Au surface. Data collection periods of only $\sim$ 2 hrs per sample were required to allow the assignment of the local environment of the Zn (with an estimated 4 hrs necessary for a more extended assignment), which are comparable to the timescales of more traditional techniques for studying the structure at the electrode/electrolyte interface. As such, XAS offers a competitive and complementary in situ technique for the structural investigation of low concentration species in the vicinity of the electrode surface.

5 Acknowledgements

The authors acknowledge the ESRF for provision of synchrotron radiation facilities and would like to thank Thomas Neisius for outstanding assistance in the operation of beamline ID26. JRIL also thanks the Engineering and Physical Sciences Research Council for financial support and Dr. Sven L.M. Schröder for helpful discussions. Portions of this work were performed under the auspices of the U.S. Department of Energy by Lawrence Livermore National Laboratory in part under Contract W-7405-Eng-48 and in part under Contract DE-AC52-07NA27344.

References

[1] D.M. Kolb, *J. Electroanal. Chem.*, **54** (1974) 25.

[2] D.M. Kolb, M. Przasnyski, H. Gerischer, *Advances in Electrochemistry and Electrochemical Engineering*; John Wiley and Sons Ltd. (1978)

[3] S. Szabó, *Inter. Rev. Phys. Chem.*, **10** (1991) 207.

[4] E. Herrero, L.J. Buller, H.D. Abruña *Chem. Rev.*, **101** (2001) 1897.

[5] S.J. Gurman, N. Binsted, I. Ross, *J. Phys. C*, **17** (1984) 143.

[6] S.J. Gurman, *J. Phys. C: Solid State Phys.*, **21** (1988) 3699.

[7] J. McBreen, *J. Solid State Electrochem.*, **13** (2009) 1051.

[8] M. Giorgetti, S. Passerini, W.H. Smyrl, S. Mukerjee, X.Q Yang, J. McBreen, *J. Electrochem. Soc.*, **146** (1999) 2387.

[9] M. Giorgetti, S. Mukerjee, S. Passerini, J. McBreen, W.H. Smyrl, *J. Electrochem. Soc.*, **148** (2001) A768.

[10] J.G. Gordon, O.R. Melroy, M.F. Toney, *Electrochim. Acta*, **40** (1995) 3.

[11] S. Wu, J. Lipkowski, T. Tyliszczak, A.P. Hitchcock, *Prog. Surf. Sci.*, **50** (1995), 227.

[12] T. Tyliszczak, A. Hitchcock, S. Wu, A. Chen, G. Szymanski, J. Lipkowski, *Synchrotron Radiat. News*, **11** (1998) 31.

[13] J.R.I. Lee, R.L. O'Malley, T.J. O'Connell, A. Vollmer, T. Rayment, *J. Phys. Chem. C*, **113** (2009) 12260.

[14] M. Nakamura, A. Aramata, A. Yamagishi, M. Taniguchi, *J. Electroanal. Chem.* **446** (1998) 227.

[15] A. Aramata, S. Taguchi, T. Fukuda, M. Nakamura, G. Horányi, *Electrochim. Acta*, **444** (1998) 999.

[16] S. Takahashi, K. Hasebe, A. Aramata, *Electrochem. Commun.*, **1** (1999) 301.

[17] S. Takahashi, A. Aramata, M. Nakamura, K. Hasebe, M. Taniguchi, S. Taguchi, A. Yamagishi, *Surf. Sci.* **512** (2002) 37.

[18] S. Moniwa, A. Aramata, *J. Electroanal. Chem.*, **376** (1994) 203.

[19] M.G. Chu, J. McBreen, G. Adzic, *J. Electrochem. Soc.*, **128** (1981) 2281.

[20] A. Manzoli, M.C. Santos, S.A.S. Machado, *Thin Solid Films*, **515** (1997) 6860.

[21] A.R. Despic, M.G. Pavlovic, *Electrochim. Acta*, **27** (1982) 1539.

[22] M.H. Fonticelli, D. Posadas, R.I. Tucceri, *J. Electroanal. Chem.*, **565** (2004) 359.

[23] A. Aramata, M.A. Quaiyyum, W.A. Balais, T. Atoguchi, M. Enyo, *J. Electroanal. Chem.*, **338** (1992) 367.

[24] M.A. Quaiyyum, A. Aramata, S. Moniwa, S. Taguchi, M. Enyo, *J. Electroanal. Chem.*, **373** (1994) 61.

[25] S. Taguchi, A, Aramata, M.A. Quaiyyum, M. Enyo, *J. Electroanal. Chem.*, **374** (1994) 275.

[26] S. Taguchi, T. Fukuda, A. Aramata, *J. Electroanal. Chem.*, **435** (1997) 55.

[27] G. Horányi, A. Aramata, *J. Electroanal. Chem.*, **434** (1997) 201.

[28] G. Horányi, A. Aramata, *J. Electroanal. Chem.*, **437** (1997) 259.

[29] S. Taguchi, A. Aramata, *J. Electroanal. Chem.*, **457** (1998) 73.

[30] L.D. Burke, T.G. Ryan, *Electrochim. Acta*, **37** (1992) 1363.

[31] A.A. El-Shafei, *J. Electroanal. Chem.*, **380** (1995) 269.

[32] K. Igarashi, A. Aramata, S. Taguchi, *Electrochim. Acta*, **46** (2001) 73.

[33] T. Boiadjieva, M. Monev, A. Tomandl, H. Kronberger, G. Fafilek, *J. Solid State Electrochem.*, **13** (2009) 671.

[34] G. Adzic, J. McBreen, M.G. Chu, *J. Electroanal. Chem.*, **128** (1981) 1691.

[35] Y.S. Lo, N.D. Huefner, W.S. Chan, P. Dryden, B. Hagenhoff, T.P. Beebe, *Langmuir*, **15**, (1999) 6522.

[36] Y. Golan, L. Margulis, I. Rubenstein, *Surf. Sci.*, **264** (1992) 312.

[37] M.G. Samant, M.F. Toney, G.L. Borges, L. Blum, O.R. Melroy, *Surf. Sci.*, **1-2** (1988) L29.

[38] E.A. Stern, *Phys. Rev. B*, **48** (1993) 9825.

[39] N. Binsted, *PAXAS: Program for the Analysis of X-ray Absorption Spectra* (1988)

[40] J.W. Cook, D.E. Sayers, *J. Appl. Phys.*, **52** (1981) 5024.

[41] N. Binsted, *EXCURV98: CCLRC Daresbury Laboratory computer program* (1998).

[42] A. Tadjeddine, D. Guay, M. Ladouceur, G. Tourillon, *Phys. Rev. Lett.*, **66** (1991) 2235.

[43] A. Tadjeddine, G. Tourillon, D. Guay, *Electrochim. Acta*, **36** (1991) 1859.

[44] A. Tadjeddine, G. Tourillon, *Sov. Electrochem.*, **29** (1993) 82.

[45] K.-O. Thiel, A. Vollmer, M. Hintze, E. Avci, C. Donner, *Z. Phys. Chem.*, **221** (2007) 1255.

[46] A. Vollmer, E. Avci, K. Thiel, C. Donner, *J. Electroanal. Chem.*, **605** (2007) 15.

[47] S. Trasatti, *J. Electroanal. Chem.*, **33** (1971) 351.

[48] H. Gerischer, D.M. Kolb, M. Przasnyski, *Surf. Sci.*, **43** (1974) 662

[49] D.M. Kolb, H. Gerischer, *Surf. Sci.*, **51** (1975) 323

[50] J. Wang, A.J. Davenport, H.S. Isaacs, B.M. Ocko, *Science*, **255** (1992) 1416.

[51] J. Wang, B.M. Ocko, A.J. Davenport, H.S. Isaacs, *Phys. Rev. B*, **46** (1992) 10321.

[52] D.M. Kolb, *Prog. Surf. Sci.*, **51** (1996) 109.

[53] K.G. Huang, D. Gibbs, D.M. Zehner, A.R. Sandy, S.G.J. Mochrie, *Phys. Rev. Lett.*, **65** (1990) 3313.